Localized fluidization in a granular medium

Pierre Philippe, M. Badiane

HAL Id: hal-02924768
https://hal.inrae.fr/hal-02924768

Localized fluidization in a granular medium

P. Philippe , M. Badiane

Irstea, UR OHAX,

3275 route de Cézanne, CS40061, Aix-en-Provence, F-13182 France

(April 4, 2013)

We present here experimental results on the progressive development of a fluidized zone in a bed of grains, immersed in a liquid, under the effect of a localized upward flow injected through a small orifice at the bottom of the bed. Visualization inside the model granular medium consisting of glass beads is made possible by the combined use of two optical techniques: refractive index-matching between the liquid and the beads and planar laser-induced fluorescence. Gradually increasing the injection rate, three regimes are successively observed: static bed, fluidized cavity that does not open to the upper surface of the granular bed, and finally fluidization over the entire height of the granular bed inside a fluidized chimney. The phase diagram is plotted and partially interpreted using a model previously developed by Zoueshtiagh and Merlen (*Physical Review E* 75, 053613, 2007). A typical sequence, where the flow-rate is first increased and then decreased back to zero, reveals a strong hysteretic behavior since the stability of the fluidized cavity is considerably strengthened during the defluidization phase. This effect can be explained by the formation of force arches within the granular packing when the chimney closes up at the top of the bed. A study of the expansion rate of the fluidized cavity was also conducted as well as the analysis of the interaction between two injection orifices with respect to their spacing.

PACS numbers: 45.70.Qj, 47.55.Lm, 47.56.+r

I. INTRODUCTION

Many natural soils are cohesive with very low permeability. Thus, they can hardly dissipate an excess of fluid pressure via a macroscopic internal flow but may be forced to fracture in cracks, giving rise to preferential flow paths connecting upstream to downstream [1,2]. Conversely, destabilization by an excess of fluid pressure is significantly different for a cohesionless soil. Indeed, under the action of the hydrodynamical forces generated by an internal flow inside an immersed granular bed, the grains have the ability to reorganize themselves collectively, either globally or at an intermediate scale, thus modifying the internal structure of the medium and subsequently the fluid flow. The archetype of such hydromechanical instabilities is fluidization, induced by an upward fluid flow within a grain packing. However, despite the large number of works dedicated to fluidized beds, only a few studies have focused on the primitive phases of initiation and development of a fluidized zone inside a granular bed, prior entire fluidization of the medium.

The situation studied is either a localized injection of fluid to force the location of a fluidized zone, either in 2-phase [3,4] or 3-phase [5,6] systems, or an homogeneous flow able, under favorable conditions, to induce vertical fluidization channels [7–9]. In both cases, the grain instability is driven at an intermediate length scale and the subsequent decrease in porosity and permeability force the water flow to intensify locally, through the fluidized sections. It is this feedback between the local granular structure and the porous flow which is responsible for the development of a fluidized chimney throughout the medium. Experimental evidence for such porosity waves has already been reported and modeled in fluidized sand column [10–12] but only for fluidization over the entire cross-section of the column. But, at present, little is known about the kinematics of fluidization when the hydro-mechanical instability is local, not global, with a localization which may be inherent or induced by forcing. The underlying scientific question is to properly understand the mechanical coupling between fluid and grains in a frictional granular medium of variable density, from concentrated suspension to consolidated porous medium [13]. Some numerical modelings have been proposed so far combining discrete and continuous approaches respectively for solid and fluid phases [14–21] but reliable experimental data at the grain scale are still scarce.

The objective of the present work is to analyze the expansion and the final steady-state of a fluidized zone initiated at the base of an immersed granular pile by a spot of upward liquid injection at constant flow rate. It should be noted that the present study on the development of a fluidized zone within a static bed differs from the general situation of fully fluidized beds in which secondary instabilities can appear, as bubbles. This topic has been studied extensively both for many practical applications but also for fundamental problems associated with it, including the role of inertial effects (see [22] and references therein) and particularly the fact that liquid-fluidized beds are inherently more stable than gas-fluidized beds [23,24].

Several industrial processes rely on such a localized state of fluidization. May be mentioned both spouted beds [25,26] and tapered beds [27] designed to several specific processes (drying, agglomeration, mixing, coating, ...) by means of an upward-gas flow. Also exist

some fluidizer systems used for the maintenance of navigable waterways [28]. On the contrary, in some other applications of fluidized bed reactors, the existence of a preferential flow path, also called channeling, should be avoided as discussed for instance in [29,30]. Development of underground cavities induced by a leak from a pipe is another major concern for industry and may, in some situations, have catastrophic consequences as was the case in February 2005 with the accident which happened to a chemical plant of the company Kemira Kemi in Helsingborg, Sweden [21,31]. The mechanical behavior of such fluidized granular slurries, straight regulated by friction [13], is also of great interest for the engineering of gas and oil recovery from poorly cemented sandstone reservoirs [11,32–34], and potentially for processes linked to CO_2 geo-sequestration. Hydraulic fracturing carried out for the extraction of shale gas [35,36] is a related example that is currently being highly debated in terms of environmental risk. Heterogeneous fluidization in growing water-filled crack is also evoked in sedimentology to account for some natural structures observed in layered sediments and consequently called "fluid-escape structures" [37–39]. Other geological issues are related to localized fluidization of a granular medium such as formation of diverging kimberlite volcano conduits (e.g. [40,41]), fluid venting in unconsolidated sea bed sediments (see for instance [5,6] and references therein). On a smaller scale, the cones of sand deposit, called "sandboils", which may appear at the downstream of a flood protection dam, are the signature of quite similar phenomena: such a localized fluidization can be initiated by a seepage flow that seeps into the foundation and then rises vertically behind the dam [42–44]. The fluidized and eroded zone can develop backward to form a pipe. Beyond a certain length of pipe, this backward erosion becomes irreversible and leads in a few hours to failure of the dam [44,45].

Direct probing within a granular medium is the main experimental difficulty when one wishes to study the specific dynamics of this type of material. A solution commonly implemented to circumvent this problem is to use a quasi two-dimensional geometry, for example by placing the grains in the gap between two parallel walls. In the case of interest here, namely that of localized fluidization, this solution has been used in several previous experimental studies such as [41,46,47] for instance. However, the problem with this type of geometry is the presence of front and back side walls, which necessarily have a significant influence on the behavior of the system, in particular through the additional friction created at the walls. To avoid this, it is obviously preferable to operate with a real, unconfined three-dimensional geometry. But this requires to probe locally the heart of a granular system and not be limited to its visible boundaries. Several techniques can be used, such as X-ray tomography or Magnetic Resonance Imaging, and a growing number of studies are based on these not intrusive techniques. Here, the choice has been made to carry out a direct visualization technique that requires a specific combination

of grains and liquid so as to adjust the refractive index of the two phases. A recent review paper about this refractive index matched scanning technique for dense granular materials can be found in [48] and a brief description is given later in the present paper. The implementation of this technique allowed us to track the development of a fluidization zone within the granular material from the injection site. A first series of results has been presented briefly in a previous paper [49]. This work is now addressed in much greater depth, with a large number of original experimental and theoretical findings.

The paper is organized as follows. Section II is devoted to the experimental aspects of this work: description of both the set-up and the two optical techniques that allow direct visualization within the granular bed, namely refractive index-matching (RIM) and planar laser induced fluorescence (PLIF). The protocol is then detailed as well as the different parameters whose influence have been tested and their respective ranges of variation. The experimental results are summarized in Section III where a phase diagram is proposed for the three regimes successively encountered when the flow rate is increased: static bed, cavity of fluidized grains, and finally chimney of fluidization throughout the bed. Is also described in this section the hysteretic behavior observed through the increased lifetime of the fluidized cavity when the flow rate is decreased back from a previous state of fluidized chimney. Additional experimental results are reported: first on the transient kinetics of upward expansion of the fluidized zone to a final stationary regime of either fluidized cavity or chimney, and second on the situation where two injection orifices are used and where an interaction between the fluidized zones can be observed. All these results are discussed in Section IV and partly interpreted by a simple theoretical model adapted from [3] and by the non-dimensionalization that follows. Finally, a summary as well as conclusions and prospects are discussed in Section V.

II. EXPERIMENTAL SET-UP

A. Optical techniques and materials

The refractive index matched scanning technique [48] which has been implemented relies on the combination of two optical techniques. The first one, Refractive Index Matching (RIM), is achieved by using liquid and solid phases of same refractive index and RIM granular medium chosen here is constituted of glass beads immersed in a mineral oil mixture. Specific characteristics and properties of the two phases will be presented hereafter. Once this matching made, the immersed granular medium becomes translucent. But this is not enough to visualize locally the internal structure of the grains and a second technique must be employed: Planar Laser Induced Fluorescence (PLIF). The principle is as follows.

Foremost, a small amount of fluorescent dye is added to the liquid phase. Then, the material is illuminated by a laser sheet in the area of interest. As a consequence, the fluorescence of the dye is excited only in this portion illuminated by the laser light which re-emits its own light with a shift in wavelength. By inserting an optical filter, it is possible to retrieve only the light emitted by fluorescence and to remove all direct light from the laser. Images of good contrast are thus obtained, on which the liquid phase appears in clear and solid phase (i.e. grains) in dark as sketched in figure 1.
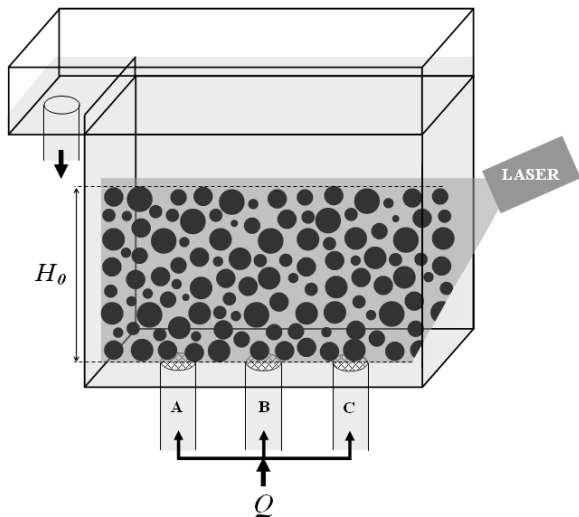
FIG. 1. Schematic of the experimental device. A layer of borosilicate glass beads, of height H_0, is placed in a rectangular cell of inner section $200 \times 80mm$, previously filled with an oil mixture of the same refractive index as the beads. A fluorescent dye added to the liquid provides a visualization in a vertical slice, within the granular system, by illuminating with a laser sheet. At the bottom of the grain layer, three injection nozzles (ports A, B and C) can be used to generate a localized flow likely to destabilize the medium. The flow rate Q is kept constant and injected by means of a gear pump and the liquid is discharged by overflow, thus maintaining a constant level at the top of the cell.

To properly implement together RIM and PLIF techniques, we made the following choices for the different materials used in our experiments, based on a previous study on another topic using the same techniques [50]. Our granular medium is constituted of spherical borosilicate beads (manufactured by SiLi) immersed in a mixture of two mineral oils in proportions chosen to adjust at best the refractive index of the mixture to that of the glass constituting the beads, namely $n \approx 1.473$. The resulting mixture is made approximately of 86% (in mass) of a light mineral oil (supplied by Sigma-Aldrich) and 14% (in mass) of a "type A" immersion oil (supplied by Cargille). This mixture has a dynamic viscosity and a density equal respectively to $\eta_m \approx 18.3 \times 10^{-3} \mathrm{kg.m.s^{-1}}$ (measured with a falling ball viscometer) and $\rho_m \approx 850 \mathrm{kg.m^{-3}}$ (measured by weigh-

ing). Three sizes of beads were successively used in these experiments with respective mean diameters of $d = 3$, 5 and 6.4mm, each batch having a substantially monodisperse size distribution. The density of these borosilicate beads is $\rho_b \approx 2230 \mathrm{kg.m^{-3}}$. The fluorescent dye required for the PLIF technique is Rhodamine 6G (supplied by Fluka) whose fluorescence can be activated by a laser at 532nm. The optical filter used to separate fluorescence re-emission from direct laser emission is a high-pass optical filter at 590nm. The laser is a 100mW green laser line generator module at 532nm (manufactured by Coherent) with a fan angle of 60° and a uniform angular distribution of intensity. The focus of the laser was adjusted so that the width of the illuminated area is not more than 0.5mm within the entire region of interest. Taking advantage of the axisymetric configuration around the vertical axis centered on the injection hole, it was not necessary here to implement a systematic scanning procedure throughout the granular medium [48] and the laser sheet is simply positioned in the vertical median plane containing the axis of symmetry and parallel to the front and back sides of a rectangular cell as can be seen in Figure 1.

B. Set-up and protocol

The experimental set-up used in these experiments is sketched in Figure 1. The cell is a rectangular plexiglass box with internal dimensions $200 \times 200 \times 80mm$ (height×length×width). Three injection ports, labeled respectively A, B, and C on the diagram of Fig. 1, are positioned at the bottom of the cell, in the median plane. They can be opened or closed independently. The distance between A and B and between B and C is the same, equal to 40mm. In most of the experiments presented here, only the central opening was used. Some additional results have been achieved in the situation where two injection openings are open simultaneously, either with a small distance between holes (injection ports B and C) or with a larger spacing (injection ports A and C).

The diameter of the injection ports is $D_1 = 14mm$ and this value can be reduced to $D_2 = 6mm$ with the addition of a perforated cylindrical piece. A perforated grid is screwed onto the base of the cell, just above the injection ports. As shown in Fig.1, an extension part was added at the top of the cell to establish a side overflow and thus to ensure a constant level of oil in the cell. Note that the rising liquid is the same than the liquid surrounding the medium.

To prepare a granular sample, a given mass of beads M ($0.25 \leq M \leq 3 \mathrm{kg}$) is poured into the cell before it is slowly filled with oil via the bottom injection holes. Finally, a glass stick planted vertically in the bead packing is moved systematically throughout the entire medium, firstly to remove any air bubbles that would have remained trapped but mostly to ensure a reproducible state

3

of compaction. Before any deformation or destabilization induced by fluid flow, the initial sample has a height H_0 and a solid volume fraction Φ.

Each experiment is carried out by imposing for a sufficiently long time an injection liquid flow at a constant rate using a gear pump (VG540 supplied by Verder). The sequence is recorded by a CCD camera (XCD-X710 supplied by Sony) at 5fps with a resolution of 1024×768pixels. The dimensions of the imaging field are approximate 13×10cm (length×height). After each sequence, the sample is homogenized with the stick to recover its initial state whenever the flow has led, or not, to a destabilization of the granular medium.

C. Parameters under focus

Several experimental series were carried out to analyze the influence of different parameters. The first of them is the bead diameter, three values were successively used: $d = 3$mm, $d = 5$mm and $d = 6.4$mm. For a given material, the control parameters are obviously H_0, the initial height of the sample, and Φ, the solid volume fraction. Both will control the material's resistance against the upward liquid flow. However, the sample preparation protocol does not allow varying the latter parameter which remains equal approximately to $\Phi \approx 0.61$ whatever the bead diameter and the height of the sample. In contrast, the initial height H_0 varies in direct proportion of the total mass of beads M. In the experiments, H_0 ranges from 1 to 13.5cm. Regarding the force imposed by the liquid flow, the flow rate Q provides most contribution and may be varied up to a maximum value close to 120cm^3.s^{-1}. In addition, the influence of the diameter of the injection holes was also studied working either with $D_1 = 6$mm or $D_2 = 14$mm. A last parameter whose influence has been tested is the spacing between injection holes, δ, in the situation where two similar injections are simultaneously used to fluidize the granular bed. Two values were used: $\delta_1 = 40$mm (injection holes B and C) and $\delta_2 = 80$mm (injection holes A and C).

III. EXPERIMENTAL RESULTS

A. Stationary regimes

1. Description

First of all, the experiments show that, for a given granular pile of height H_0, three stationary regimes are successively encountered depending on the flow rate transiting through the injection hole.

(i) *Static regime:* Except a very small sample expansion at initial pressurization, the granular layer remains immobile during all the sequence with imposed flow rate.

(ii) *Cavity regime:* A fluidization zone develops just above the injection hole but is restricted to a cavity of fluidized grains which does not extend to the top of the sample. Only the grains into the cavity are moving along a turbulent convection roll, somewhat similar to within a washing machine.

(iii) *Chimney regime:* The fluidization zone quickly reaches the top of the sample thereby creating a chimney of fluidized grains. The steady-state is obtained from a balance between the upward flux of grains carried out by the flow in the central part of the chimney and the downward flux of outlying avalanches that continuously refuel the system.

The different pictures presented in Figure 2 illustrate the above observations. For all three regimes, in this image is presented first an individual image (Fig.2a, e, i) as well as the average image of the granular system in its steady state (Fig.2b, f, j). Note in all the images the small dark rectangle at the center-bottom of the frame. It is due to a screw head located between the laser plane and the camera which therefore does not obstruct the flow and can precisely locate the injection hole. The following images (Fig.2c, g, and k) are obtained in two steps (performed with the free image processing program ImageJ): (1) subtraction of the previous average image to images of the sequence, (2) projection retaining only the brightest pixels of the entire sequence. A clearer area is emerging where grain motion is observed. Thanks to this image processing, we can distinguish unambiguously between steady states (ii) and (iii) where the grains are mobilized only within a cavity (Fig.2g), whose height is noted h_f, below an almost immobile granular roof or inside a chimney (Fig.2k) that perforates the entire grain layer upwards. Finally, the last illustrations (Fig.2c, g, k) are spatiotemporal diagrams that show the time evolution within the dotted area (768pixels high and 50pixels wide, centered on the injection hole) in which the pixels were averaged along the horizontal lines. When fluidization occurs, these diagrams show the initial development and expansion of the fluidized zone until a steady regime is reached which is either a cavity (Fig.2h) or a chimney (Fig.2l). A final way to differentiate regimes (ii) and (iii) is achieved when comparing an individual image (Fig.2e, i) of the steady-state to the average one (Fig.2f, j). There are few differences between these two images in the case of the fluidized cavity since only the grains inside the cavity are in motion. Conversely, there is a significant difference in the fluidized chimney regime where a large blurred area is observed around the chimney flue. The boundary of this area coincides exactly to the one revealed by the image processing undergone by Fig.2k. It corresponds, as was already said, to a downward motion of grains which is almost similar to a surface avalanche and feeds continuously with grains the fluidized chimney.
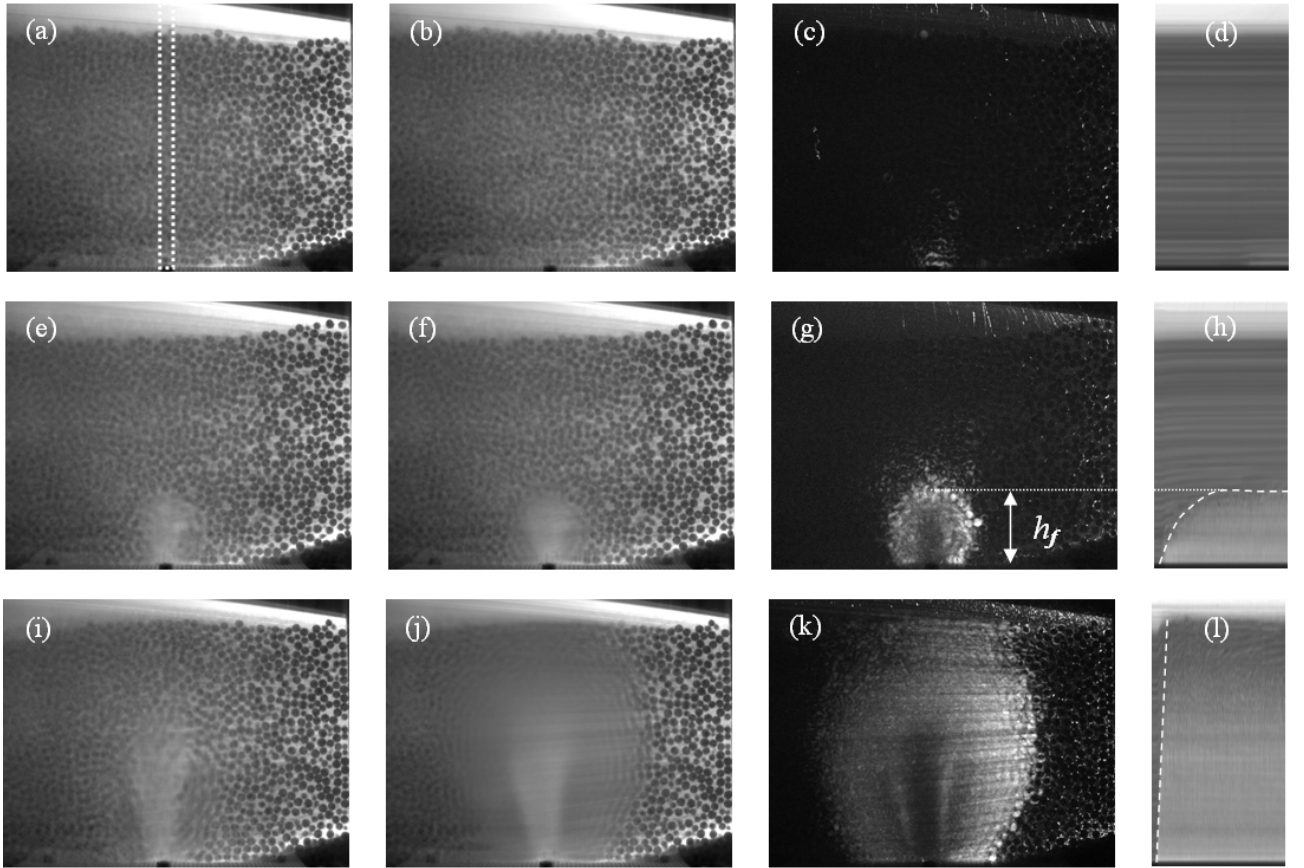
FIG. 2. Illustration of the three different steady states for a 5mm-bead layer of initial height $H_0 = 12.0$cm and with an injection hole $D_2 = 14$mm: (i) Static regime ($Q = 69.5$cm^3.s^{-1}; images a, b, c, and d); (ii) Fluidized cavity regime ($Q = 86.9$cm^3.s^{-1}; images e, f, g and h); (iii) Fluidized chimney regime ($Q = 100.8$cm^3.s^{-1}; images i, j, k and l). The two first sets of images are respectively an individual picture (images a, e, and i) and the average image (images b, f, and j) in each of the three steady states. The next series of pictures (images c, g, and k) is obtained after subtraction of the average image then projection retaining only the brightest pixels of the entire sequence. The last pictures are spatio-temporal diagrams plotted from the vertical lines centered on the injection hole and contained in the dotted rectangle shown in image a.

2. Hysteresis behavior

Let us denote Q_{cav} and Q_{chim} the critical flow rate values at the boundaries respectively between the static regime and the cavity regime, and between the cavity regime and the chimney regime. To accurately estimate these values, h_f, the average height of the fluidized zone, can be plotted as a function of the flow rate Q. This is shown in Figure 3 for a 5mm-bead layer with an initial thickness of $H = 12.0$cm. As can be seen, h_f gradually increases with Q in the fluidized cavity regime and the threshold Q_{cav} is quite easily determined by extrapolating h_f to zero. The subsequent transition from cavity to chimney regime, when h_f reaches H, allows here again to measure precisely the second threshold Q_{chim}. Beyond this value, h_f becomes equal to the total height of the fluidized chimney, H, which gets about 20 to 30% greater than the initial height H_0 owing to the local dilatancy of the layer related to the intense convective motion of grains.

Substantially the same curve is obtained when subjecting this time, the initial layer to a unique sequence of fluidization with successive stages of constant injection flow rate at increasing intensity. But, when decreasing back the flow rate intensity by a reverse sequence, a totally different behavior is observed. Indeed, where the fluidized cavity would collapse rapidly when decreasing flow rate, we observe instead that it remains in place for much lower flow rates than the one for which it first appeared, namely Q_{cav}. More precisely, an abrupt decrease is first observed for the fluidized height h_f due to the closure of the chimney at the top of the granular layer. This closure occurs at a flow rate Q_{clo} almost equal to Q_{chim}. Then, the height of the cavity decreases regularly and almost linearly with the flow rate. The final collapse takes place only at a very low flow rate, denoted Q_{col}, which can be 3 or 4 times smaller than Q_{cav}. It is important here to underline this surprising difficulty to heal in a granular medium after prior hydraulic fracturing by a fluidized chimney. From a practical point of view in the field of civil protection against flooding, it means that a

5

sand-boil which appeared during a crisis situation only closes back superficially, whereas, deeper in the structure, it can remain active for a much longer duration. As will be detailed and discussed further in Section IV, this very pronounced hysteresis effect can be explained by the creation of arches in force chains between grains when the fluidized chimney closes back. The upper grain layer which comes to rest finds support on the static area, at the periphery of the fluidized zone, which acts as an abutment.
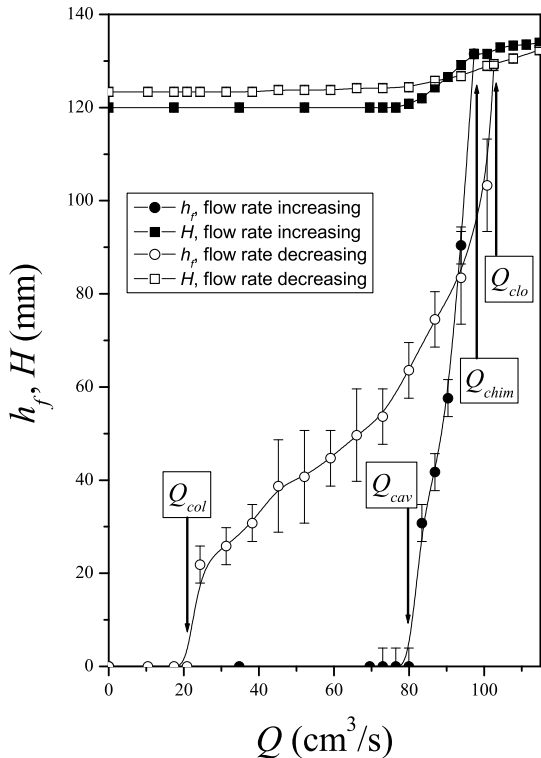
FIG. 3. Plot of both (circle symbols) h_f, the height of the fluidized zone, and (square symbols) H, the total height of the layer in vertical alignment with the injection hole for a 5mm-bead layer of initial height $H_0 = 12.0$cm and with an injection hole $D_2 = 14$mm. A hysteresis effect is seen by comparing the measurements obtained during a sequence of increased flow rate (solid symbols) and a sequence of decreased flow rate after prior chimney fluidization (open symbols). The critical flow rate values successively encountered in an increase-decrease sequence are noted respectively: Q_{cav} (first occurrence of a fluidized cavity), Q_{chim} (creation of a fluidized chimney), Q_{clo} (back closure of the fluidized chimney), and Q_{col} (final collapse of the fluidized cavity). The solid lines are only guides for the eyes.

3. Phase diagram

The dependency of Q_{cav}, Q_{chim}, and Q_{col} on the initial sample height H_0 can be accounted for through the construction of a phase diagram in the $H - Q$ plane. To do this, the steady state reached in each experiment for an initial height H_0 and imposed flow rate Q is reported in the diagram. Note also that no distinction is made here between Q_{chim} and Q_{clo}, the onset respectively of chimney first occurrence and back closure, whose values are very close. The complete diagram obtained for 5mm-beads and a 6mm-diameter injection hole is shown in Figure 4.
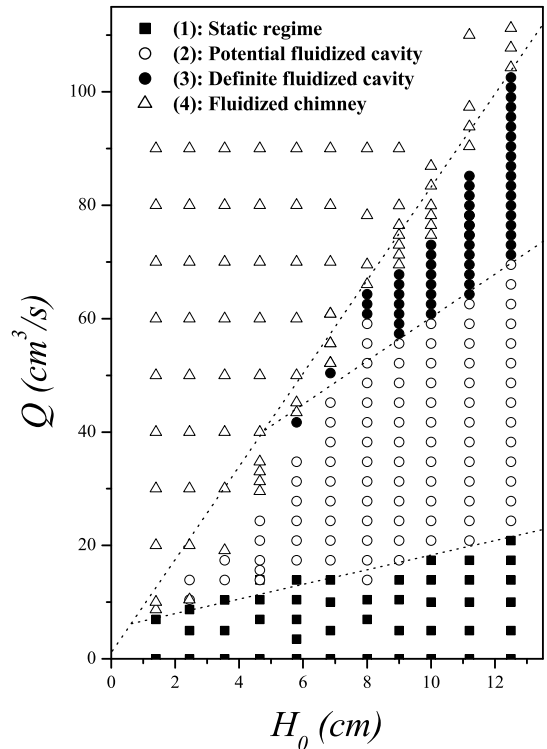
FIG. 4. Phase-diagram summarizing the different steady-states observed when a flow rate Q is injected at the base of a bead layers of initial height H_0, here with 5mm-beads and an injection hole $D_1 = 6$mm. The four regimes are: (1) Static regime (solid square symbols); (2) Potential fluidized cavity regime (open circle symbols); (3) Definite fluidized cavity regime (solid circle symbols); (4) Fluidized chimney regime (open triangle symbols). The dotted lines are only guides for the eyes.

This phase-diagram corresponds to about 250 separate realizations and can distinguish the following 4 domains.

(1) $Q < Q_{col}(H_0)$: Static regime.
(2) $Q_{col}(H_0) < Q < Q_{cav}(H_0)$: Potential occurrence of a fluidized cavity.
(3) $Q_{cav}(H_0) < Q < Q_{chim}(H_0)$: Definite occurrence of a fluidized cavity.
(4) $Q > Q_{chim}(H_0)$: Fluidized chimney regime.

As already explained above, a fluidized cavity is actu-

ally observed in domain (2) if and only if domain (4) has been reached beforehand by the system. Otherwise, the granular layer remains static.

An important finding concerns the boundaries between these domains, given respectively by the relations $Q_{col}(H_0)$, $Q_{cav}(H_0)$, and $Q_{chim}(H_0)$. From Fig.4, one can notice that they all have a rather linear dependence with height H_0, especially the onset of fluidized chimney which, as can be also seen in Figure 5, is compatible with a law of the form:

$$Q_{chim}(H_0) = Q_0 \left(1 + \frac{H_0}{\Delta}\right) \qquad (1)$$

where Q_0 and Δ are respectively a flow rate and a length reference value whose physical interpretation will be given later.
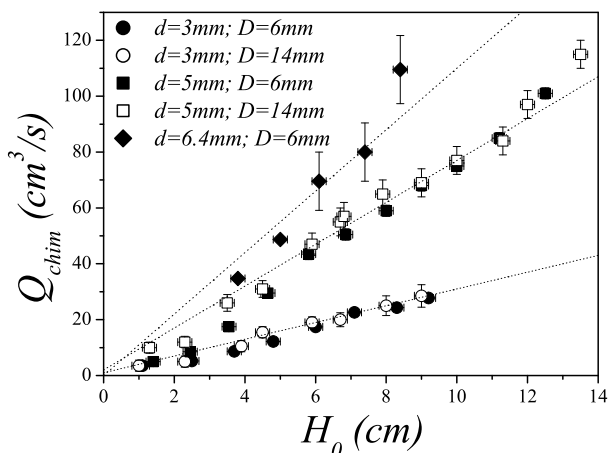
FIG. 5. The critical flow rate Q_{chim} at the onset of fluidized chimney as a function of the initial height H_0 for several experimental series with bead diameter respectively equal to $d = 3$mm ($\circ$, $\bullet$), $d = 5$mm ($\square$, $\blacksquare$), and $d = 6.4$mm ($\blacklozenge$), and with two different sizes of the injection hole, $D_1 = 6$mm (solid symbols) and $D_2 = 14$mm (open symbols). The dotted lines are only guides for the eyes.

In Fig.5, Q_{chim} is plotted as a function of H_0 for different values of bead size ($d = 3$mm, $d = 5$mm, and $d = 6.4$mm) and injection hole diameter ($D_1 = 6$mm and $D_2 = 14$mm). The objective here is to test the possible influence of these two parameters. And, from Fig.5, the answer is as follows: the fluidized chimney threshold depends clearly on the bead diameter but substantially not on the size of the injection area. However, this latter conclusion must be modulated as the range of variation of D explored here is limited. Intuitively, it is likely that an influence will be felt for significantly higher values of D. Dependence with d is through an increase in Q_{chim} with the grain diameter. As will be detailed in Section IV, this effect can be interpreted simply by the fact that, rather than flow rate, the pressure gradient is the

source of destabilization. Then, according to Darcy's law and knowing that permeability is related to the square of the grain diameter, a strong dependence with d (a priori quadratic) must obviously be found.
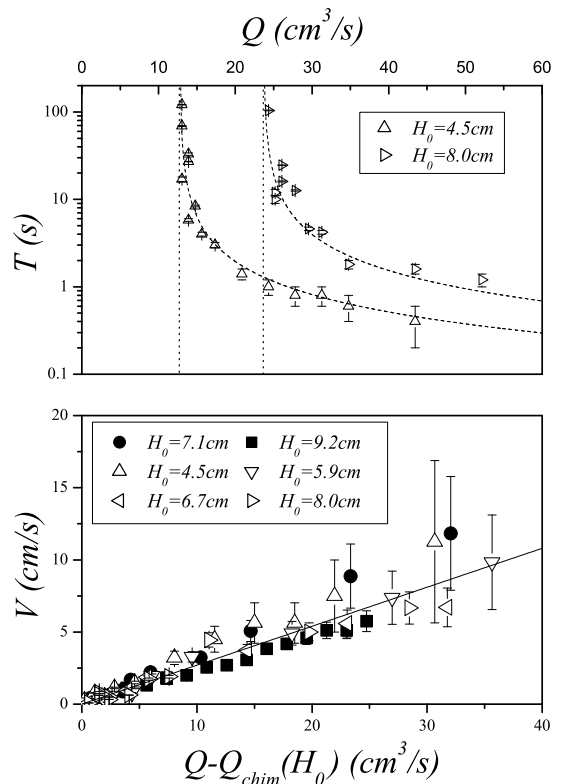
FIG. 6. (Up): Duration T of the upward expansion phase of the fluidized zone, from initiation to establishment of the chimney regime, as a function of flow rate Q with 3mm-beads and injection hole $D_2 = 14$mm, and for initial height $H_0 = 4.5$cm ($\triangle$) and $H_0 = 8.0$cm ($\triangleright$). The vertical dotted lines are the two asymptotes $Q = Q_{chim}(H_0)$ and the dashed curves are of the form: $T \propto (Q - Q_{chim})^{-1}$. (Down): Global expansion rate $V = H_0/T$ versus excess flow rate $Q - Q_{chim}(H_0)$ with injection holes $D_1 = 6$mm (solid symbols) and $D_2 = 14$mm (open symbols) and for $H_0 = 7.1$cm ($\bullet$), $H_0 = 9.2$cm ($\blacksquare$), $H_0 = 4.5$cm ($\triangle$), $H_0 = 5.9$cm ($\triangledown$), $H_0 = 4.5$cm ($\triangleleft$), $H_0 = 8.0$cm ($\triangleright$). The solid line stands for Eq.(3) with $A = 0.27$cm^{-2}.

B. Transient regimes to steady fluidized state

As could already be noticed in the spatio-temporal diagrams of Fig.2, the steady states of fluidized cavity and chimney are preceded by a transient phase, more or less long, during which the fluidization zone is first initiated at the injection hole then extends gradually, and mainly upward, to the rest of the medium. Systematic measurements of the duration of this phase of upward expansion were carried out in the fluidized chimney regime. Typical

results are shown in Figure 6.

The dependency of T with flow rate shows a sharp divergence when Q tends to Q_{chim}; this divergence is nicely accounted for by a power law of the type:

$$T(Q, H_0) \propto \left(Q - Q_{chim}(H_0)\right)^{-1} \qquad (2)$$

In this latter equation, the proportionality coefficient is obviously a function of H_0. To further investigate this relationship, we can define a global expansion rate, V, as the ratio between the sample height H_0 and the duration T. This quantity, plotted against the excess flow rate $Q - Q_{chim}(H_0)$, shows, as expected, a linear dependency with a new proportionality coefficient, A, which appears this time to be independent of the height H_0 as shown in Fig.6:

$$V(Q, H_0) = \frac{H_0}{T(Q, H_0)} = A\left(Q - Q_{chim}(H_0)\right) \qquad (3)$$

For the beads with diameter $d = 3$mm, this coefficient is approximately equal to $A_{d=3mm} \approx 0.27 \pm 0.02$cm^{-2}. Note from Fig.6 that this finding is the same for both injection hole sizes which confirms the independence of all the results with D, at least in the range investigated in the present study.

In contrast, coefficient A is different for the experiments performed with 5mm beads. The results are somewhat more scattered and provide the following estimate: $A_{d=5mm} \approx 0.16 \pm 0.04$cm^{-2}.

C. Interaction between two chimneys

The last series of experiments carried out in the course of this study concerns the situation where there is no more a single injection hole but two identical nozzles separated by an horizontal gap δ. Depending on whether ports B and C or ports A and C are open, two values of δ have been used: $\delta_1 = 40$mm and $\delta_2 = 80$mm. The diameter of injection was meanwhile kept constant, equal to $D_1 = 6$mm and the flow rate Q refers to the total flow distributed through both injection holes.

The objective here is to analyze the possibilities of interaction between two fluidized zones. This question has received very few attention in the literature, both from a fundamental point of view or in the context of the different geological and industrial applications presented in the introduction to this work. To our knowledge, in this specific situation where several locally fluidized areas coexist in a granular environment, there seems to be only a few studies, all obtained for the configuration of spouted beds (see for instance [51] and references therein).

Specifically, what is observed is that two fluidized chimneys sufficiently far from each other seem to have individual behavior similar to the single chimney case without visible interaction between fluidized zones. On the contrary, if the injections are moved towards one another, the transient regime is strongly disturbed: the fluidized cavities which develop above each injection hole attract each other and eventually merge to generate almost a single chimney conduit. This is illustrated in Figure 7, for a 3mm-bead layer of initial height $H_0 = 9.2$cm and a total flow rate Q just above the chimney regime threshold, where is clearly observed the interaction and fusion between fluidized pipes for $\delta_1 = 40$mm while two separate chimneys grow almost independently in the case where $\delta_2 = 80$mm.
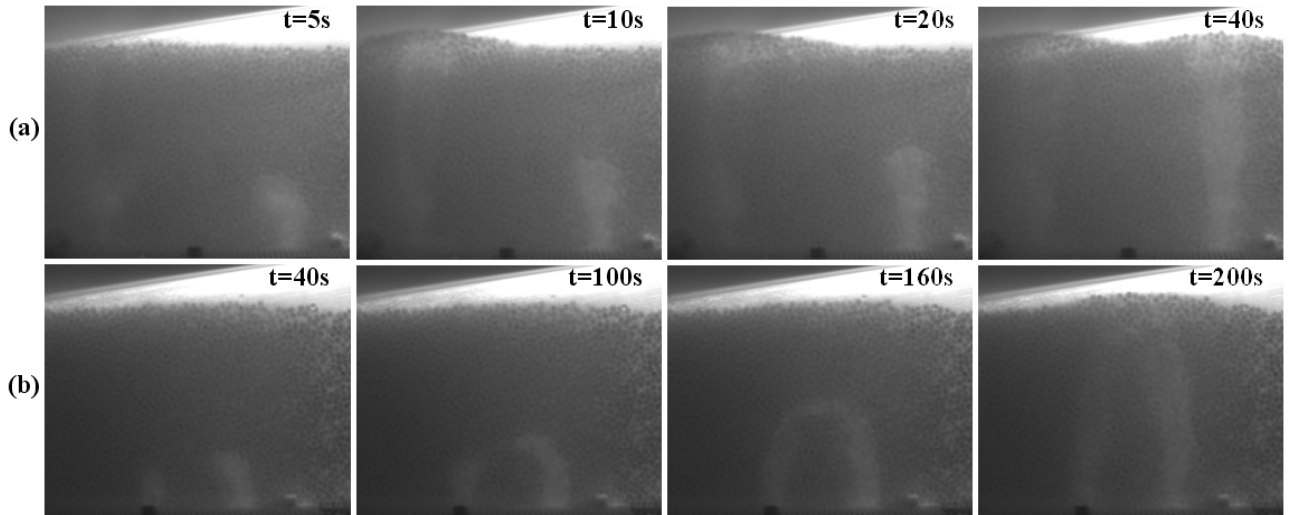
FIG. 7. Successive stages in a sequence of fluidization of a 3mm-beads layer of initial height $H_0 = 9.2$cm by two injection holes spaced by δ and with a constant flow rate Q taken juts above the fluidized chimney regime: (a) $\delta = \delta_2 = 80$mm and $Q = 45.2$cm^3.s^{-1}; (b) $\delta = \delta_1 = 40$mm and $Q = 29.6$cm^3.s^{-1}

This interaction can also be quantified in terms of Q_{chim}, the critical flow rate for initiation of the fluidized chimney regime. Thus, for example, in the configuration of the Fig.7, $Q_{chim}^{2h}(\delta_1) \approx 29\mathrm{cm}^3.\mathrm{s}^{-1}$ and $Q_{chim}^{2h}(\delta_2) \approx 44\mathrm{cm}^3.\mathrm{s}^{-1}$ were found respectively in the cases with and without interaction. Compared with $Q_{chim}^{1h} = 27.4 \pm 0.3\mathrm{cm}^3.\mathrm{s}^{-1}$, the value obtained for a single injection hole, a threshold slightly less than twice this value is logically recovered for $\delta = \delta_2$. This shows that each localized fluidization seems to be almost independent of its neighbor provided that it is far enough away. Instead, for two injection holes close enough to interact and merge their fluidized cavities, the critical flow remains practically unchanged with respect to the single injection hole case. There is therefore a very effective and almost perfect sharing of the two upward jet flows. In summary, the critical flow rate for fluidized chimney is determined by the final number of chimneys and not by the prescribed number of injections. Note, however, that a larger gap between $Q_{chim}^{2h}(\delta_1)$ and Q_{chim}^{1h} was found in experiments with 5mm-beads.

As can be noted in Fig.7, the duration of the transient is much longer in the case of interacting fluidized cavities. This can be explained by the flow rate that is much lower in this case. With regard to the cases where the interaction between fluidized area is limited, one can see that once the first chimney is formed (indifferently at the left or the right injection), the transient regime gets significantly slowed. For instance, in the experiment presented in Fig.7, the transient to fluidized chimney lasted less than 10s for the left injection but about 40s for the right one. Presumably, as soon as the first chimney is created, a small amount of flow rate coming from the other injection hole is deviated towards the chimney. This greatly slows down the duration of the transient for the remaining cavity and may even prevent the formation of the second chimney. Note that the value Q_{chim}^{2h} is taken as the onset for two fluidized chimneys and not for a intermediate situation with a chimney and a cavity.

What we present here are only preliminary results obtained on a small number of experiments with different values of the initial sample height. Moreover, with our device, there are only two possible values for the distance between the two injection holes. We plan in the short run a full study of the interaction between chimneys, with an adjustable distance between the injection nozzles and analyzing both situations with two but also three or more injection holes.

IV. DISCUSSION

A. A model for fluidized chimney threshold

To interpret the value of the initiation threshold of a fluidized chimney Q_{chim}, we follow here the model proposed by Zoueshtiagh and Merlen [3]. The idea is to decompose the flow in two parts. The first one corresponds to the flow generated throughout the porous medium from the small injection at its base. As long as the flow is far from the walls and upon the assumption that the injection is nearly punctual, the situation is similar to that of a point source in a semi-infinite porous medium. In this latter case, with the additional assumption that the flow in the granular bed obeys Darcy's law, the flow rate can be simply calculated as a function of the pressure gradient and is denoted Q_{ps}. This calculation was reasonably well validated by some experimental measurements [3].

Then it is assumed that, besides the homogeneous porous flow rate Q_{ps}, a second contribution must be added to account for the upward flow that generates fluidization inside the chimney. The previous experimental observations have shown that the fluidization zone, which we called chimney, had a roughly cylindrical shape as measured by Zoueshtiagh and Merlen [3] or as can also be seen in Fig.2(i-k). Assuming therefore a cylindrical shape for this chimney, with a diameter noted λ, as well as a vertical homogeneous flow through a section $\Sigma = \pi/4\lambda^2$, the related fluidization flow rate Q_{hf} is easily calculated according to the pressure gradient.

Finally, by equating for both flow contributions the pressures at the injection hole and at the upper surface of the granular layer, it comes, after some calculations which are detailed in [3], that the threshold flow rate for the onset of fluidized chimney can be written as:

$$Q_{chim} = Q_{ps} + Q_{hf} = Q_{hf}\Big(1 + 4\frac{H_0}{\lambda}\Big) \qquad (4)$$

The theoretical prediction given by this equation can account for the scaling law proposed in Eq.(1) for the linear dependence of Q_{chim} with the initial bead layer height H_0. As a consequence, Δ and Q_0 coincide respectively with $\lambda/4$ and Q_{hf}. This latter parameter can be calculated analytically based on Darcy's law with a permeability k. Here we use for k the empirical expression derived from the Carman-Kozeny formula in the case of a sphere packing [52]: $k = (1 - \Phi)^3 d^2/(180\Phi^2)$ where Φ is the solid volume fraction and d the bead diameter. As the fluidization threshold is obtained when the pressure gradient balances exactly the immersed weight of the grains, Q_{hf} reads:

$$Q_{hf} = \Sigma \frac{k}{\eta_m}\Big(\frac{\Delta P_f}{H_0}\Big) = \frac{\pi\lambda^2}{4} \frac{(1 - \Phi)^3 d^2(\rho_b - \rho_m)g}{180\Phi\eta_m} \quad (5)$$

where η_m is the viscosity of the liquid while ρ_b and ρ_m are respectively the solid and liquid density.

The only unknown parameter in Eq.(5) is the chimney diameter λ. However, based on our experimental observations and the ones reported by Zoueshtiagh and Merlen [3], it is expected that λ does not depend, or very little, on both the injection diameter D and the bead diameter d. Therefore, there is a priori no obvious reference length in the system for the chimney width. As a consequence, the use of a dimensionless form is not appropriate but we

can still introduce the following reference section σ that accounts for bead size and fluid properties:

$$\sigma = \frac{180\Phi\eta_m Q}{(1-\Phi)^3 d^2(\rho_b - \rho_m)g} \qquad (6)$$

From Eq.(4) and Eq.(5), it comes that chimney fluidization occurs in a bead layer of height H_0 when σ is greater than:

$$\sigma_{chim}(H_0) = \frac{\pi}{4}\lambda^2\Big(1 + 4\frac{H_0}{\lambda}\Big) \qquad (7)$$

To test this relationship, the data in Fig.5 are now plotted in Figure 8 showing σ_{chim} as a function of H_0.
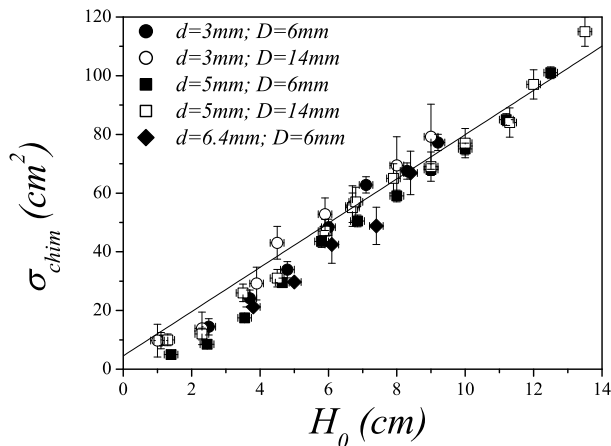
FIG. 8. Critical value of the characteristic section σ_{chim} at the onset of fluidized chimney as a function of the initial height H_0 for several experimental series with bead diameter respectively equal to $d = 3$mm ($\circ$, $\bullet$), $d = 5$mm ($\square$, $\blacksquare$), and $d = 6.4$mm ($\blacklozenge$), and with two different sizes of the injection hole, $D_1 = 6$mm (solid symbols) and $D_2 = 14$mm (open symbols). The best fit to Eq.(7) is given by the solid line with $\lambda = 24$mm.

This figure shows, on the one hand, that the use of σ_{chim} instead of Q_{chim} produces a nice collapse of all data, and, on the other hand, that a satisfactory agreement is obtained with respect to the theoretical prediction given by Eq.(7). The adjustment provides for the fluidized chimney diameter $\lambda \approx 24$mm which seems quite reasonable compared to the related pictures in Fig.2 and to some previous measurements of the chimney radius by Zoueshtiagh and Merlen [3].

Obviously this low value of λ cannot remain the same when wider injection holes are considered and the independence of λ with respect to D observed in the present study is valid only for sufficiently small injection areas, presumably for $D \lesssim \lambda$. Beyond, λ should certainly increase with D.

Similarly, although in the range studied here, λ does not seem to depend on the grain size d, we should reasonably expect an increase of λ with d. However, judging by

the present results with $d = 3$, 5 and 6.4mm, this influence of the grain diameter does not seem to be observed for $\lambda > 4d$.

One last point about this characteristic fluidization length scale λ concerns the interaction between two chimneys as reported in Section III C. Indeed, considering two vertical chimneys of diameter λ, located just above the injection holes separated each other by a distance δ, the width of the static zone situated in-between the two fluidized chimneys is equal to $l = \delta - \lambda$. The observations made in Section III C show that the fusion between two separate fluidized cavities seems to occur when l is in the range of λ, that is to say when $\delta \sim 2\lambda$. This is particularly visible for the two sequences shown in Fig.7 where we have precisely $\delta_1 < 2\lambda < \delta_2$. In other words, in the direct vicinity of a fluidized zone, a static area can remain stable only if its size is greater than λ which can be regarded as the minimum length of stability with respect to fluidization.

B. Fluidized cavity and hysteresis

To our knowledge, this is the first time that a fluidized cavity regime is experimentally highlighted. This state was predicted and briefly discussed by Zoueshtiagh and Merlen [3] but not observed in their experiments. Somewhat similar porosity waves have been previously reported but for homogeneously, rather than locally, fluidized sand column [10–12]. Meanwhile on the side of numerical simulation, this cavity regime was only very recently modeled [21] but without a real comprehensive study of it. The present work provides new results on the fluidized cavity regime concerning: i) the strong hysteresis effect on fluidized cavity existence when comparing increasing/decreasing flow rate sequences; ii) the upward expansion rate of the fluidized area during the transient regime. The latter point concerns the transients leading to a final fluidized steady state which can be either a cavity or a chimney and will be discussed further in Section IV C. Here, we focus on the hysteresis effect of the fluidized cavity which was highlighted in our experiments (see Section III A 2 and Fig.3).

When referring to a hysteresis effect in the context of fluidization, one may rather recall the slight difference observed between the fluidization and the defluidization thresholds. This is a well established result from the experimental point of view which is mainly explained by the internal friction of the particle bed. This influence of friction was for instance reported and discussed by Zoueshtiagh and Merlen [3], and a very comprehensive theoretical study has been proposed by Jackson [53] for fluidization and defluidization in a particle bed.

As underlined by our experiments on the existence of the fluidized cavity regime, a completely different and original type of hysteresis effects is observed here. Indeed, the observations of Section III A 2 show that the

domain of existence of a fluidized cavity, which is quite limited when the flow rate is gradually increased, becomes considerably extended when the flow rate is reduced back. As already mentioned, we believe that this rather spectacular effect is mediated by friction which allows creating an arch at the bottom of the static top layer that forms at the defluidization threshold when some grains begin to immobilize at the surface while the whole bottom area remains fluidized. The action of this arch is added to that of the flow and thus puts the system in a state of mechanical stability to flow rates far much lower than those responsible for the initial fluidization of the granular medium. When drag force and friction can no more balance the overlying burden, the cavity ultimately collapses at a flow rate Q_{col} as previously defined in Section III A 2.
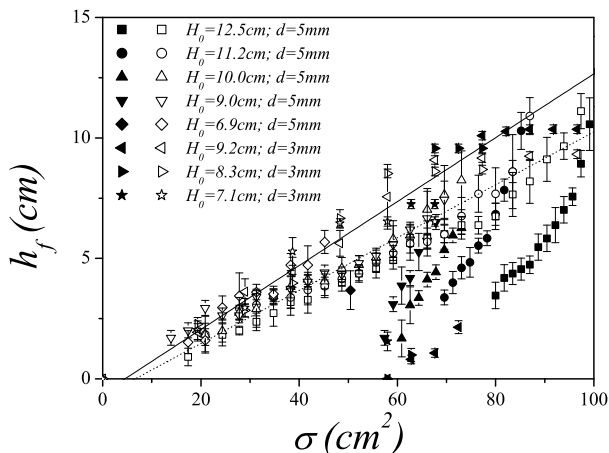
FIG. 9. Height h_f of the fluidized cavity versus σ during increasing (solid symbols) and decreasing (open symbols) flow rate sequences for an injection hole $D = 6mm$, for two bead diameters ($d = 3mm$ and $d = 5mm$) and with several values of the initial height H_0: $d = 5mm$ and $H_0 = 12.5cm$ (square symbols), $H_0 = 11.2cm$ (circle symbols), $H_0 = 10.0cm$ (up triangle symbols), $H_0 = 9.0cm$ (down triangle symbols), $H_0 = 6.9cm$ (lozenge symbols); $d = 3mm$ and $H_0 = 9.2cm$ (left triangle symbols), $H_0 = 8.3cm$ (right triangle symbols), $H_0 = 7.1cm$ (diamond symbols). The solid and dotted lines stand for Eq.(8) with respectively $\lambda = 24mm$ and $\lambda = 29mm$.

In the light of the model presented above, it is possible to test this interpretation. For this, suppose that during the defluidization process a vault is created, reorienting partially the weight of the upper layer to the lateral areas of the sample that remained static. The height of the fluidized cavity located below the arch is noted h_f. If this vault is strong enough to retain completely the top of the bed with the combined action of the upward flow, the upper part thus plays no role with respect to the fluidized area. We can therefore consider that the situation is equivalent to that of a fluidized chimney in a bed of

height h_f. The flow rate is exactly the one corresponding to the fluidized chimney threshold for h_f and we can write $Q = Q_{chim}(h_f)$ or, indifferently, $\sigma = \sigma_{chim}(h_f)$. Replacing H_0 by h_f and $\sigma_{chim}(H_0)$ by σ in Eq.(7), the following relationship between h_f and σ:

$$ h_f = \frac{\sigma}{\pi\lambda} - \frac{\lambda}{4} \tag{8} $$

When plotting the height h_f of the fluidized cavity during a defluidization sequence as the function of σ, one can see on Fig.9 that there is almost a collapse of all the data obtained with several initial sample heights H_0 and two different bead diameters. As can be seen in Fig.9, the prediction given by Eq.(8) using for λ the value found in the previous section, namely $\lambda = 24mm$, is quite close to the experimental data while an even better agreement is obtained for a slightly larger value of λ: $\lambda = 29mm$.

C. Transient regime

Whatever the final steady state reached by the system, namely fluidized cavity or fluidized chimney, the transitory situation is that of a fluidized cavity in upward expansion. In our experiments, the typical value of the upward growth rate is given by V as reported in Section III B with data obtained only for a final system with a steady fluidized chimney.

Following the theoretical developments of Section IV A, the same scaling relation can be tested for this expansion rate V. For this, as is shown in Figure 10, the data of Fig.6 as well as similar ones obtained for $d = 5mm$ are plotted against $\sigma - \sigma_{chim}(H_0)$.
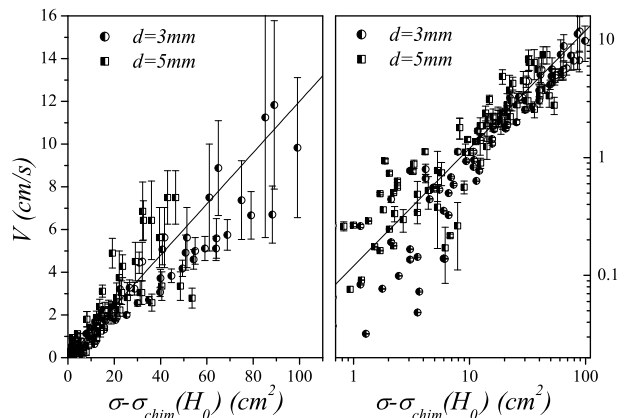
FIG. 10. Expansion rate $V = H_0/T$ plotted versus $\sigma - \sigma_{chim}(H_0)$ in linear-linear and log-log representations for all the data obtained with bead diameters $d = 3mm$ and $d = 5mm$ for both injection holes $D_1 = 6mm$ and $D_2 = 14mm$. The solid line stands for Eq.(9) with $a = 0.1cm^{-1}.s^{-1}$.

11

Here again, a rather good collapse is observed but with more scattering due to larger error bars when measuring the duration of the transient regime. The linear relation is kept and reads now:

$$V = a\Big(\sigma - \sigma_{chim}(H_0)\Big) \tag{9}$$

The adjustment shown in Fig. 10 provides approximately $a \sim 0.1 \text{cm}^{-1}.\text{s}^{-1}$.

For a comparison in a situation exactly similar, there is, to our knowledge, only one proposal in the related literature, by Zoueshtiagh and Merlen [3] who suggest considering the upward expansion of the fluidized zone as the passage of a kinematic shock wave, characterized by a discontinuity between a fluidized and a non-fluidized state. Following this reasoning, a simple proportionality relationship is predicted between V and Q, in disagreement with our results (see Fig.6) and with the empirical law given by Eq.(3).

In the broader context of fluidized beds, there are theoretical expressions to describe kinematic as well as dynamic waves, able to propagate in such systems [53,54]. A theoretical analysis of kinematic porosity waves was also developed by Vardoulakis [12]. The same kind of expression as the one proposed by Zoueshtiagh and Merlen is recovered for a kinematic shock velocity. For a dynamic wave velocity, a simple, but controversial, expression is proposed by Gibilaro [54]. However, this law does not predict any variation with Q and therefore cannot explain the behavior observed here, for the localized fluidization.

To go further in the discussion, two significant differences should be highlighted between the specific case of localized fluidization and the more general framework of fluidized beds within which these theories have been developed. First of all, there is no homogeneous water discharge at the bottom of the particle bed as for fluidized beds and the problem can no more be considered as a unidimensional one. The validity of the theoretical expressions obtained in this 1D approximation can therefore be questioned for localized fluidization. Moreover, unlike the case of propagating waves in a fluidized bed, the porosity contrast here is between a fluidized zone (cavity) and a top layer of motionless grain that remains almost static. This last point indicates that the interactions between grains are very different: rather than collisions between fluidized particles there exists permanent contacts between grains inside the upper layer above the cavity and the main grain-grain interactions are frictional type. Moreover, the specific geometry of the cavity, with a rather small characteristic diameter λ, amplifies the role of friction between grains by promoting the creation of arches at the top of the cavity. These vaulted structures strengthen the mechanical resistance and may stabilize very substantially the static upper layer of the granular bed. Consequently we believe that arching, which already explains the hysteresis effect on the domain of existence of a fluidized cavity as was discussed in the previous section, is also responsible for the very long duration of the transient regime observed in the experiments (see Fig.6) when the flow rate is only slightly larger than its critical value for chimney fluidization. On the contrary, far enough above this threshold, friction induced stability is too weak for slowing down fluidization; the upward expansion of the fluidized zone is therefore very fast and much more similar to an usual kinematic wave.

If we focus more specifically on the slow transient regimes, the movies obtained from the experiments reveal that the cavity is the location of a highly turbulent flow with a wide vortex occupying substantially all of the cavity and driving the fluidized grains in its movement. The "ceiling" of the cavity, consisting of grains in contact, is stressed by this particle laden vortex and may ultimately destabilize. Thus some grains feed the fluidized cavity while a new arch forms. In this context, the upward expansion of the cavity can be seen as a succession of vault destabilizations at the top of the fluidized area. It may be noted here some similarity, both formal and conceptual, with erosion of grain sediment. And indeed, the expansion rate V can be related to the most commonly used law for sediment erosion [55,56] which can be written as follows:

$$E = \beta \frac{\tau - \tau_c}{\rho_s - \rho_f} \tag{10}$$

where E is the erosion rate (in m.s^{-1}), β is a proportionality coefficient (in m^{-1}.s), τ is the shear stress exerted by the fluid on the sediment (in kg.m^{-1}.s^{-2}), τ_c is the sediment resistance to erosion (in kg.m^{-1}.s^{-2}), ρ_s is the sediment density (in kg.m^{-3}), and ρ_f is the fluid density (in kg.m^{-3}). The density difference $\rho_s - \rho_f$ characterizes the loss of mass per unit volume induced by erosion of the sediment that is replaced by the fluid..

A relation almost similar to Eq.(10), but written at a more global scale, can be obtained for the expansion rate V. Noting from Eq.(7) that $\sigma_{chim}(H_0)$ is very close to $\pi\lambda H_0$ when H_0 becomes large compared to λ (typically for $H_0 > 5$cm), another way to express V can be proposed and reads from Eq.(5), Eq.(6) and Eq.(9):

$$V = b\frac{\Delta P - \Delta P_f}{\rho - \rho_m} \tag{11}$$

where ΔP is the overall pressure drop through the part of the sample corresponding to the final fluidized chimney, ΔP_f is the minimum pressure drop for homogeneous fluidization in a sample of height H_0 as defined in Eq.(5), and $\rho = \Phi\rho_b + (1 - \Phi)\rho_m$ is the bulk density.

The relationship between b and a reads simply:

$$b = \frac{\pi a \lambda}{g} \sim 7.7 \times 10^{-4} \text{cm}^{-1}.\text{s} \tag{12}$$

In Eq.(11), the expansion rate V is now directly related to the momentum created by the excess of pressure drop. Roughly similarly to sediment erosion, this resultant momentum is dissipated by turbulent rolls in

the cavity, which, as already suggested above, gradually destabilize the motionless grains at the top of the cavity and thus contribute to upward expansion of the fluidized area by grain loss at the upper static layer in favor of the cavity.

V. SUMMARY AND PROSPECTS

A granular layer, subjected to an ascending flow from a small injection hole at constant flow rate, destabilizes locally and forms a fluidized cavity in upward expansion. Depending on the magnitude of the flow rate, the resulting steady situation consists either of a cavity or of a chimney when the fluidized zone pierces the whole height of the granular bed.

The latter stationary regime requires a minimum flow rate which depends linearly on the initial height of the sample. Expending a previous model by Zoueshtiagh and Merlen [3], a theoretical prediction can account very satisfactorily for this result and also offers a more general scaling that integrates fluid viscosity, buoyancy, grain size and initial volume fraction of the sample.

For lower flow rates, the fluidized zone remains localized inside the sample. The domain of existence of these stationary fluidized cavities is quite limited as long as the threshold for chimney onset is not reached. But it is greatly extended if, juste prior, the system has first reached the fluidized chimney regime. This hysteresis effect is well marked and can be satisfactorily interpreted by assuming that, at defluidization, a temporary arch is creating and maintained at the roof of the fluidized cavity. Benefiting from the additional action of the fluid flow, this vault manages to stabilize the cavity structure on a very wide range.

The study of the transient regime, during which the fluidization gradually spreads from the injection zone to the upper free surface, showed that the characteristic rate of expansion was proportional to the deviation to the threshold for fluidized chimney onset. Some similarity with the laws of sediment erosion has been highlighted and discussed.

At last, preliminary results in the situation where the upward fluid flow transits through two separate injections show that a significant interaction can be felt when the gap between the two injections is small enough and favors the emergence of a single chimney after mutual attraction of the two fluidized cavities originally created.

To our opinion, the present work needs to be continued for at least two points. Firstly, the results regarding the interaction between two chimneys are limited at this stage and it would be very interesting to conduct a more comprehensive study on this subject, in particular to continuously vary the gap between the two sources and also to analyze more complex situations with three competing sources. We planned for soon an experimental work accordingly. Secondly, to analyze the local mechanisms responsible for fluidization and grain destabilizations with greater precision than is possible with the experiments, we have developed a numerical model to describe such systems where grains interact with a fluid flow. This work is in progress and the first results will be presented quite shortly.

[1] E.G. Flekkøy, A. Malthe-Sørenssen and B. Jamtveit, Journal of Geophysical Research **107**(B8), ECV1 (2002).
[2] D.F. Boutt, L. Goodwin, B.J.O.L. McPherson, Water Resources Research **45**(5), W00C13 (2009).
[3] F. Zoueshtiagh and A. Merlen, Physical Review E **75**(5), 056313 (2007).
[4] A. Nermoen, O. Galland, E. Jettestuen, K. Fristad, Y. Podladchikov, H. Svensson and A. Malthe-Sørenssen, Journal of Geophysical Research **115**, B10202 (2010).
[5] G. Varas, V. Vidal and J.-C. Géminard, Physical Review E **83**(1), 011302 (2011).
[6] G. Varas, V. Vidal and J.-C. Géminard, Physical Review E **83**(6), 061302 (2011).
[7] T. Wilhem and K. Wilmanski, International Journal of Multiphase Flow **28**, 1929-1944 (2002).
[8] P. Rigord, A. Guarino, V. Vidal and J.-C. Géminard, Granular Matter **7**(4), 191-197 (2005).
[9] A. Nermoen, C. Raufaste, S.D. de Villiers, E. Jettestuen, P. Meakin and D.K. Dysthe, Physical Review E **81**, 061305 (2010).
[10] I. Vardoulakis, M. Stavropoulou and A. Skjaerstein, Philosophical Transactions of the Royal Society of London, Series A-Mathematical Physical and Engineering Sciences **356**, 2591-2608 (1998).
[11] E. Papamichos, I. Vardoulakis, J. Tronvoll and A. Skjaerstein, International Journal for Numerical and Analytical Methods in Geomechanics **25**, 789-808 (2001).
[12] I. Vardoulakis, Geotechnique **54**(2), 117-130 (2004).
[13] B. Sandnes, E.G. Flekkøy, H.A. Knudsen, K.J. Måløy and H. See, Nature Communications **2**, 288 (2011).
[14] B.K. Cook, D.R. Noble and J.R. Williams, Engineering Computations **21**(2-4), 151-168 (2004).
[15] N.G Deen, M. van Sint Annaland, M.A. Van der Hoef and J.A.M. Kuipers, Chemical Engineering Science **62**, 28-44 (2007).
[16] U. El Shamy and M. Zeghal, Soil Dynamics and Earthquake Engineering **27**(8), 712-729 (2007).
[17] Y.T. Feng, K. Han and D.R.J. Owen, International Journal for Numerical Methods in Engineering **72**(9), 1111-1134 (2007).
[18] D.F. Boutt, B.K. Cook, B.J.O.L. Mac Pherson and J.R.

Williams, Journal of Geophysical Research **112**, B10209 (2007).

[19] J.J. Derksen, Physics of Fluids **23**, 113303 (2011).

[20] L. Goren, E. Aharanov, D. Sparks and R. Toussaint, Pure and Applied Geophysics **168**, 2289-2323 (2011).

[21] X. Cui, J. Li, A. Chan and D. Chapman, Particuology **10**, 242-252 (2012).

[22] D.L. Koch and R.J. Hill, Annula Review of Fluid Mechanics **33**, 619-647 (2001).

[23] P.N. Segre and J.P. Mc Clymer, Journal of Physics-Condensed Matter **16**(38), S4219-S4230 (2004).

[24] Y.A. Sergeev, D.C. Swailes and C.J.S. Petrie, Physica A **335**, 9-34 (2004).

[25] J.M. Link, L.A. Cuypers, N.G Deen and J.A.M. Kuipers, Chemical Engineering Science **60**, 3425-3442 (2005).

[26] V.S. Sutkar, N.G. Deen and J.A.M. Kuipers, Chemical Engineering Science **86**, 124-136 (2013).

[27] Y. Peng and L.T. Fan, Chemical Engineering Science **54**(4), 2277-2290 (1997).

[28] R.N. Weismann and G.P.Y. Lennon, Journal of Waterway, Port, Coastal, Ocean Technology **41**(2), 233-253 (1994).

[29] M. Leva, M. Weintraub, M. Grummer, M. Pollchik and H.H. Storch, Bulletin 504, Bureau of Mines, US Gov. Printing Office, Washington (1951).

[30] L.A. briens, C.L. Briens, A. Margaritis, S.L. Cooke and M.A. Bergougnou, Powder technology **91**, 1-9 (1997).

[31] M. Söderlund, P. Bots, P. Eriksson, P. Nilsson and J. Hartlen, Loss Prevention Bulletin - Institution of Chemical Engineers **195**, 22-27 (2007).

[32] A. Nouri, H. Vaziri, H. Belhaj and R. Islam, SPE Journal **11**(2), 227-237 (2006).

[33] D.F. Boutt, B.K. Cook and J.R. Williams, International Journal for Numerical and Analytical Methods in Geomechanics **35**, 997-1018 (2010).

[34] R. Mourgues, J.B. Gressier, L. Bodet, D. Bureau and A. Gay, Marine and Petroleum Geology **28**, 1111-1121 (2011).

[35] K.D. Mahrer, Journal of Petroleum Science **24**(1), 13-28 (1999).

[36] M.M. Rahman and M.K. Rahman, Energy Sources Part. A-Recovery Utilization and Environmental Effects **32**(15), 1416-1436 (2010).

[37] D.R. Lowe, Sedimentology **22**(2), 157-204 (1975).

[38] R.J. Nichols, R.S.J. Sparks and C.J.N. Wilson, Sedimentology **41**(2), 233-253 (1994).

[39] T. Mörz, E.A. Karlik, S. Kreiter and A. Kopf, Sedimentary Geology **196**, 251-267 (2007).

[40] A.L. Walters, J.C. Philipps, R.J. Brown, M. Field, T.M. Gernon, G. Stripp and R.S.J. Sparks, Journal of Volcanology and Geothermal Research **155**, 119-137 (2006).

[41] T.M. Gernon, M.A. Gilbertson, R.S.J. Sparks and M. Field, Journal of Volcanology and Geothermal Research **174**, 49-56 (2008).

[42] J.B. Sellmeijer and M.A. Koenders, Applied Mathematical Modelling **15**(6), 646-651 (1991).

[43] C.S.P. Ohja, V.P. Singh and D.D. Adrian, Journal of Hydraulic Engineering **129**(7), 511-518 (2003).

[44] V.M. van Beek, H. Knoeff and J.B. Sellmeijer, European Journal of Environmental and Civil Engineering **15**(8), 1115-1137 (2011).

[45] S. Bonelli and N. Benahmed, International Journal of Hydropower and Dams **18**(3), 94-98 (2011).

[46] G.A. Bokkers, M. van Sint Annaland and J.A.M. Kuipers, Powder Technology **140**, 176-186 (2004).

[47] W. Zhong and M. Zhang, Chemical Engineering Science **60**, 315-327 (2005).

[48] J.A. Dijksman, F. Rietz, K.A. Lőrincz, M. van Hecke and W. Losert, Review of Scientific Instruments **83**, 011301 (2012).

[49] P. Philippe and M. Badiane, Advances in Bifurcation and Degradation in Geomaterials, Editors S. Bonelli, C. Dascalu and F. Nicot, Springer, 125-129 (2011).

[50] R. Béguin, P. Philippe and Y.-H. Faure, Journal of Hydraulic Engineering, **139**(1), 1-11 (2013).

[51] M.S. van Buijtenen, W.-J. van Dijk, N.G. Deen, J.A.M. Kuipers, T. Leadbeater and D.J. Parker, Chemical Engineering Science **66**, 2368-2376 (2011).

[52] J. Bear, Dynamics of Fluids in Porous Media, American Elsevier (1972).

[53] R. Jackson, The Dynamics of Fluidized Particles, Cambridge University Press (2000).

[54] L.G. Gibilaro, Fluidization Dynamics, Butterworth-Heinemann (2001).

[55] E. Partheniades, Journal of the Hydraulics Division, ASCE, **91**, 105-139 (1965).

[56] R. Ariathurai, K. Arulanandan, Journal of the Hydraulics Division, ASCE, **104**(2), 279-283 (1978).

14